HHS Public Access

Evidence for dynamics in proteins as a mechanism for ligand dissociation

Mary J. Carroll[1], **Randall V. Mauldin**[2], **Anna V. Gromova**[1], **Scott F. Singleton**[1], **Edward J. Collins**[2,3], and **Andrew L. Lee**[1,2,*]

[1]Division of Chemical Biology and Medicinal Chemistry, Eshelman School of Pharmacy, University of North Carolina at Chapel Hill, Chapel Hill, NC 27599

[2]Department of Biochemistry and Biophysics, University of North Carolina at Chapel Hill, Chapel Hill, NC 27599

[3]Department of Microbiology and Immunology, School of Medicine, University of North Carolina at Chapel Hill, Chapel Hill, NC 27599

Abstract

Signal transduction, regulatory processes, and pharmaceutical responses are highly dependent upon ligand residence times. Gaining insight into how physical factors influence residence times, or k_{off}, should enhance our ability to manipulate biological interactions. We report experiments that yield structural insight into k_{off} for a series of eight 2,4-diaminopyrimidine inhibitors of dihydrofolate reductase that vary by six orders of magnitude in binding affinity. NMR relaxation dispersion experiments revealed a common set of residues near the binding site that undergo a concerted, millisecond-timescale switching event to a previously unidentified conformation. The rate of switching from ground to excited conformations correlates exponentially with K_i and k_{off}, suggesting that protein dynamics serves as a mechanical initiator of ligand dissociation within this series and potentially for other macromolecule-ligand systems. Although $k_{conf,forward}$ is faster than k_{off}, use of the ligand *series* allowed for connections to be drawn between kinetic events on different timescales.

A long-sought goal in the biochemistry of receptor-ligand interactions is to gain an understanding of what molecular forces contribute to binding affinity and kinetics. A fundamental question is, how does dissociation occur once a ligand (e.g., peptide or small molecule) is bound to its receptor? This is an important question since ligand residence times control the strength of regulatory processes[1–2]. One model for dissociation is simple diffusion of ligand from the receptor. A more mechanistic reasoning would be that a specific

*To whom correspondence should be addressed: A.L.L., University of North Carolina, Division of Medicinal Chemistry and Natural Products, Eshelman School of Pharmacy, Beard Hall, CB# 7568, Chapel Hill, NC 27599-7568. drewlee@unc.edu, Phone: 919-966-7821, Fax: 919-843-5150.

event physically disrupts the interaction between ligand and receptor, leading to ligand release or ejection. Indeed, myoglobin requires structural deformations to bind and release oxygen[3–4]; however, this can be viewed as a special case since ligand is completely buried from solvent. We postulate that protein structural fluctuations could be a more generally utilized mechanism for weakening intermolecular interactions and effectively 'pushing' or shearing a ligand away from its receptor. Experimental studies directed at this question should benefit structure-based drug design and protein (enzyme) engineering. From a biological perspective, because signal transduction is driven by countless cycles of ligand binding and release[5], insight into mechanisms of ligand release could also make possible the drawing of fundamental connections between internal protein dynamics and cell signaling.

To probe the potential role of dynamics in small molecule ligand dissociation, we took a 'medicinal chemistry' approach of observing how protein motions change in response to varying structural features within a ligand series. Enzymes are common pharmaceutical targets and exhibit considerable dynamics that are amenable to characterization by NMR relaxation dispersion[6–11]. Thus, to test our approach, we characterized relaxation dispersion in *E. coli* dihydrofolate reductase (DHFR) in complex with eight different antifolate inhibitors spanning an affinity range of six orders of magnitude. Three of these were reported previously: methotrexate (MTX), trimethoprim (TMP), and **1** [5-((4-chlorophenyl)thio)quinazoline-2,4-diamine][12–13] (Fig 1a). This dataset comprises a 'dynamics structure-activity relationship' (DSAR) series. In other words, this approach probes whether the dynamics of DHFR are sensitive to structural differences in small molecule ligands. As part of this series, five tetrahydroquinazoline inhibitors were designed to bind with reduced affinity for the purpose of loosening the ligands to allow detection of rare motions related to ligand dissociation. Although the location and rate of μs-ms conformational switching in DHFR depends on specific ligand structure, a cluster of residues around the active site dynamically samples the same excited state in all eight of the complexes. From the analysis of relaxation dispersion curves, the kinetics of conformational switching in DHFR were found to correlate with both K_i and k_{off}, though the conformational switching was always faster than k_{off}. These data implicate a common dynamic mechanism for dissociation of ligands within this series, and suggest that internal protein motion may be a critical event for ligand dissociation in general. The medicinal chemistry approach taken allows focused and methodical perturbations within the active site; this is in stark contrast to global systematic perturbations such as temperature variations or the addition of chemical denaturants. Recent studies have linked conformational dynamics with catalytic timescales through coincidental values of rate constants [8,14]. We show here – through use of a ligand series – that linkages can also be made between events on different timescales.

RESULTS

Antifolate series spans a large range of K_i and k_{off}

From a previous study of the dynamics of DHFR in the presence of the high affinity (K_i 1 nM) inhibitors MTX and TMP (Fig. 1a and Supplementary Fig. 1a–b), both inhibitors elicited the same pattern of slow motion in the enzyme[12]. We wondered whether that same pattern of dynamics would be observed for any inhibitor bound to the same site, regardless

of binding affinity or chemical structure. To address this question, a series of substrate-competitive DHFR inhibitors, or antifolates, with K_i values greater than 1 nM was designed. This series is comprised of five tetrahydroquinazoline-2,4-diamine compounds (compounds **2–6**, Fig. 1b). Compounds **2**, **3**, **4**, and **6** are constitutional isomers and differ only in the placement of the methyl substituent on the tetrahydroquinazoline (THQ) ring. These compounds were prepared as racemic mixtures of methyl *R* and *S* forms. Inhibitor **5** lacks the methyl substituent and thus serves as a non-enantiomeric reference. Compounds **3** and **4** were previously identified as competitive inhibitors of DHFR from a high-throughput screen of 50,000 small molecules[15]. We postulated that **2**, **5**, and **6** would have K_i values similar to those published for **3** and **4** on the basis of structural similarity. As with the three previously studied high affinity inhibitors (MTX, TMP, and **1**)[12–13], binding, structural, and dynamics properties were characterized for the THQ inhibitors in the presence of cofactor NADPH.

K_i values for the THQ inhibitors ($K_{i,app}$ in the case of racemic mixtures) were determined to confirm previous measurements[15] and to establish values for the new compounds. The K_i values cover a range of two orders of magnitude (0.3 – 43 μM, see Table 1), and the THQ compounds, as well as **1**, are named according to increasing $K_i/K_{i,app}$ (i.e., **1** is the strongest inhibitor and **6** the weakest). Overall, the methyl substituent contributes positively to the binding affinity, as evidenced by **2–4** having significantly lower $K_{i,app}$ than the K_i of **5**. Surprisingly, the methyl group at the C5 position of **6** increases $K_{i,app}$ by > 40-fold relative to **2–4**. The low apparent affinity of **6** relative to **2–5** is discussed in Supplementary Methods. From this analysis of binding affinities, it is clear that DHFR is very sensitive to minor changes in bound ligand structure.

Next, the binding kinetics for the THQ series were determined. The off-rate (k_{off} or $k_{off,app}$) for each inhibitor was determined using competitive stopped-flow fluorescence measurements. The series was found to span two orders of magnitude in k_{off} (0.2 – 20 s^{-1}), similar to the trend in K_i (Table 1). In fact, the relationship between K_i and k_{off} for these five antifolates is linear (Fig. 1c). The calculated kinetic on-rates for the THQ series are similar, in the range of $3 \times 10^5 – 3 \times 10^6$ M^{-1}s^{-1}. In the context of the entire antifolate series (MTX, TMP, and **1–6**), K_i spans a range of 10^6, k_{off} spans 10^5, and k_{on} spans 10^2. It therefore follows that, given $K_i = k_{off}/k_{on}$ and k_{on} has relatively little variation within the ligand series, binding affinity is determined largely by the rate of dissociation. Within the THQ series alone, the effect of k_{off} on K_i is larger than k_{on}, but k_{off} is less dominant than when considering all eight antifolates.

To test whether the precise *R* or *S* methyl orientation had a significant influence on binding, we separated the enantiomeric forms of **3**. We found that the two forms had k_{off} values that differed by 1.6-fold, suggesting that *R* and *S* forms are essentially indistinguishable. This is further supported by the observation that HSQC spectra of the complex formed from the racemic mixture did not show peak doublings, which would be expected if **3***R* and **3***S* have differential influence on DHFR.

Structural differences induced by the series are minimal

In characterizing the protein dynamics of a series of receptor-small molecule complexes, any structural differences must be considered, as large changes can underlie differences in observed dynamics. Large structural changes in DHFR were not expected, given the chemical similarity of the antifolates. High-resolution crystal structures were determined for E:NADPH:**3**, E:NADPH:**4**, and E:NADPH:**5** in the $P2_12_12_1$ space group (Fig. 2a and Supplementary Table 1). As expected, the overall structures are highly similar (largest backbone rmsd = 0.28 Å). The THQs bind in the folate binding pocket of DHFR, which forms a small crevice in the structure but is not closed off by the protein. We note that for the C6 methyl substituent of **3**, electron density was apparent for only one enantiomer (*R*) (Supplementary Fig. 2a), which could be due to a number of factors, such as the subtle difference in off-rate (see above). It is also possible that the *S* form also crystallized and that *R* and *S* methyls are not resolvable given the resolution of this structure (2.09 Å), although we view this as unlikely. In contrast to E:NADPH:**3**, electron density for both *R* and *S* forms in the E:NADPH:**4** structure were observed (Supplementary Fig. 2b). The slight differences in sugar puckers resulted in *R* and *S* methyl groups occupying the same space (Supplementary Fig. 2b). Regardless of the enantiomers present, the THQs overlay very closely with one another (Fig. 2a). In addition, the 2,4-diamine moieties of **3–5** overlay closely to that of MTX[16–17], although the orientation is slightly tilted such that the saturated ring of the THQs shift ~1 Å towards the side chain of Phe31.

Subtle differences in the protein structure are observable in helix C above the antifolate binding site, in the loop that follows helix C, and at N23 in the Met20 loop. The orientation of helix C is particularly noteworthy, since plasticity of this helix appears to accommodate the binding of various ligands, as noted previously[17]. Tilting of the C-terminus of this helix away from the antifolate binding site was identified previously in the presence of **1** (and NADPH), which contains a bulky and flexible side chain[13]. When overlaying the current three structures (PDB IDs 3R33, 3QYL, and 3QYO) with previously determined inhibitor complexes E:NADPH:**1** and E:NADPH:MTX (PDB IDs 3KFY and 1RX3), we find that the C-terminus of helix C is tilted away from the antifolate binding site in E:NADPH:**3** and E:NADPH:**1**, whereas it is positioned closer to the antifolate binding site in E:NADPH:**4** and E:NADPH:**5** (Fig. 2b). In the case of **3**, the *R* methyl substituent at C6 is oriented towards the helix, forcing it away. By contrast, the methyl substituents at C7 in **4** are directed away from the helix, and there is no methyl in **5**, allowing the C helix to move closer to these antifolates. The position of helix C in E:NADPH:MTX is intermediate between the shifted extremes of complexes **1**/**3** and **4**/**5** (Fig. 2b). While this helix orientation appears to be sensitive to bound antifolate structure, it does not correlate with K_i of the bound antifolate.

Unlike the structure of E:NADPH:**1** determined previously[13], the ternary complexes with **3**, **4**, and **5** show strong electron density within the Met20 loop. The loop was modeled in the closed conformation, similar to that observed in the presence of MTX. The closed Met20 loop conformation is also observed in solution for all five ternary complexes based on NMR chemical shift perturbations (CSPs) (Supplementary Fig. 2c). In all three crystal structures, strong electron density is observed for NADPH and bound antifolates (Fig. 2a and

Supplementary Fig. 2a–b). Ligand orientations were also confirmed to be identical in solution as assessed by CSPs (Supplementary Fig. 2d–e). Based on these and the above considerations, no significant differences in structure are observed among these five ternary complexes. A straightforward comparison of differential dynamics of complexes in this series is therefore possible.

Slow timescale dynamics structure-activity relationships

By registering changes in DHFR's dynamics as inhibitor structure is varied, dynamics structure-activity relationships (DSAR) are obtained. For each of the five THQ complexes, μs-ms motion was detected by ^{15}N Carr-Purcell-Meiboom-Gill (CPMG)-relaxation dispersion experiments[18]. The dynamics of DHFR on this timescale have been shown to occur as a sequence of loop motions important to catalytic function when bound to endogenous ligands[8]. In addition, interesting differences in slow motions are observed in binary complexes that are off the enzyme's catalytic cycle (E:folate, E:dihydrofolate) compared to the 'on-cycle' binary product complex (E:tetrahydrofolate), confirming the enzyme's innate sensitivity to different ligands[19]. Relaxation dispersion experiments allow for the determination of the transverse relaxation rate due to conformational exchange (R_{ex}), which is a component of the overall rate of transverse relaxation (R_2):

$$R_2 = R_2{}^o + R_{ex}, \quad (1)$$

where $R_2{}^o$ is the intrinsic transverse relaxation rate in the absence of exchange. Assuming a two-state exchange process, these experiments provide kinetic, thermodynamic, and structural information about the transition: R_{ex} depends on the exchange rate constant (k_{ex}), the populations of ground state A and excited state B (p_A and p_B), and the difference in chemical shift between states A and B (ω)[20].

In contrast to the high similarity of μs-ms dynamics that result from MTX or TMP binding[12] (Supplementary Fig. 1a–b), the THQ inhibitors elicit a more heterogeneous distribution of sites showing R_{ex} (Fig. 3 and Supplementary Fig. 3). However, among the eight complexes there are twelve consensus residues with slow motions (discussed below). Thus, the pattern of slow motion elicited by MTX and TMP is not restricted to high-affinity antifolates. In addition to the consensus 'antifolate sites', new motions are detected near the hinge region (residues 38 and 88) and in α-helices C and F as K_i increases. Although within the THQ series there appears to be no significant correlation between K_i and number of sites with R_{ex}, as a whole this series has a greater amount of R_{ex} compared with MTX and TMP. None of the motions in the series are suspected to be the result of association-dissociation cycle effects, as k_{off} values are slow (Table 1) and complexes are saturated to 99.5%.

As highlighted in previous NMR studies of the enzyme, the chemical shifts of a group of ~20 residues report directly on the conformation of the Met20 loop[21]. These 'marker' residues have distinct chemical shifts when the loop samples either the closed or occluded conformation. In the E:NADPH:**6** complex, significant R_{ex} is observed at Met20 loop switching markers, suggestive of a functional conformational switch from closed to occluded[21]. However, only five sites show a correlation between ω fitted from relaxation dispersion and δ for closed-to-occluded motion of the loop (Supplementary Fig. 4i;

residues 12, 115, 118, 120, and 149). While the loop appears to be mobile, its motion is not as clear and coherent as observed previously in the presence of **1** (13 sites in the correlation)[13]. We believe this Met20 loop motion to be the result of steric clash between nicotinamide of NADPH and the C5 methyl group of **6** within the active site (see Supplementary Methods). Residues within the F–G and G–H loops are the best ^{15}N markers of Met20 loop switching (e.g., 115, 116, 118, 119, 120, 121, 122, 149, and 150), not those within the Met20 loop itself. It should be noted that the [15]N Met20 loop marker residues within the F-G and G-H loops are not generally observed to undergo μs-ms motion in the presence of compounds **2–5** of the series (Supplementary Tables 2 and 4) and that even the best examples of closed complexes (with bound MTX or TMP) exhibit exchange broadening at some of the marker residues. In further support of E:NADPH:**6** being different from the other complexes regarding its Met20 loop mobility, G121 is severely broadened in the presence of **6** but not for the remaining compounds of the series.

Rate of conformational switching correlates with K_i and k_{off}

Residue-grouped fitting of relaxation dispersion data can indicate which sites move together in a single, concerted exchange process[22]. Residues that are included in a group fit are forced to share single k_{ex} and p_A values, whereas they retain their individual ω values. To probe whether the observed R_{ex} values reflect concerted conformational exchange processes, group fits were carried out for all of the ternary THQ complexes. For **3**, **5**, and **6**, group fitted k_{ex} values were found to range from 1000–1500 s^{-1}, which are greater than those for the higher affinity antifolates (400–800 s^{-1}), and p_B remained fixed at approximately 2% (Table 1). It follows that the forward rate of conformational exchange ($k_{conf,forward}$) ranges from 20–35 s^{-1} for these three complexes. Initial plots of $k_{conf,forward}$ versus K_i suggested a correlation for these three protein-inhibitor complexes. To further test this correlation, $k_{conf,forward}$ and K_i for MTX, TMP, and **1** were added to the plot (Tables 1 and 2)[12–13,23]. For these six complexes, covering six orders of magnitude in binding affinity, we find that $k_{conf,forward}$ correlates exponentially with K_i (Fig. 4a). As binding affinity decreases (larger K_i), $k_{conf,forward}$ increases (Table 1). Unfortunately, single-group fitting for complexes **2** and **4** did not converge and thus are not further supportive of this trend, although an alternative fit for **4** was obtained (see Methods). Based on the exponential relationship between $k_{conf,forward}$ and K_i and the linear correlation between K_i and k_{off} (Fig. 1c), $k_{conf,forward}$ vs. k_{off} was plotted and found to correlate exponentially (Fig. 4b). We note that $k_{conf,forward}$ is always greater than k_{off} by at least a factor of two for each complex, providing further evidence against k_{ex} resulting from association-dissociation cycles. This correlation of $k_{conf,forward}$ and k_{off}, with $k_{conf,forward} > k_{off}$, is highly suggestive of a mechanistic role for the ground-to-excited state conformational change in ligand release. In Figure 4b, because k_{off} for TMP and **1** are too slow for detection via the assay employed, they were calculated from K_i and their approximate k_{on} value for the series. The k_{off} value for MTX was taken from the literature[24]. The best fitted $k_{conf,forward}$ for **4** has been included in Figure 4b, even though group fitting was more challenging in this case; its position off the main correlation line suggests that additional factors may contribute to release for a particular ligand, even if it is part of a structurally constrained series. Nevertheless, the fact that the remaining ligands fall on the line suggests that the millisecond structural fluctuations potentiate dissociation over the entire ligand series, including MTX and TMP.

Antifolate complexes sample the same excited state

Relaxation dispersion experiments can also provide structural information about the excited state. As mentioned previously, from data on the eight drug/inhibitor complexes, there are ~twelve consensus residues undergoing µs-ms motion (Fig. 5a). We define a residue as a consensus site if slow motion is detected at that position (when assignable) in (a) 2/3 of the eight complexes (residues 8–11, 14, 29, 31, 111–113), or (b) ½ of the complexes when R_{ex} is significant in the other half but lies just below our stringent requirement of 2 s^{-1} (residues 7 and 30). A number of these sites were initially identified from the least dynamic complexes, those with MTX or TMP bound[12]. The dynamic change in chemical shift (ω) at these consensus sites fitted from relaxation dispersions for each complex were analyzed. For each individual residue, the fitted ω parameter clusters around the same value, despite changes in chemical structure and binding affinity for the different inhibitors (Fig. 5b). This clustering of ω values indicates that the same excited state is being sampled by the consensus residues in each of the eight antifolate complexes. This pattern of ω values does not correlate with ω fitted from previous studies of DHFR bound to physiological, folate-derived ligands (Supplementary Fig. 4j)[8] and hence is unique to the antifolates studied here. In addition, because poor correlations between ω fitted from the dispersion data and δ from chemical shift changes (E:NADPH – E:NADPH:antifolate) were observed for the consensus sites (Supplementary Fig. 4a–h), the antifolates appear to be bound in the excited state. We propose that these residues sampling a novel excited state mediate dissociation of antifolate ligand. This state is sampled at somewhat different rates, but the concerted motion of the consensus residues is conserved across these antifolate complexes.

We note that while these complexes share this common dynamic sampling, differences in slow motions remain among the complexes[12–13] (Fig. 3, Supplementary Table 2). Thus, this shared motion appears to be able to exist in the context of additional motions (or lack thereof) in other regions of the enzyme.

DISCUSSION

Binding and dissociation are the two fundamental processes that determine a ligand's affinity for its receptor. Mechanistic insight into these processes is therefore expected to facilitate rationale design of drugs and macromolecules with desired ligand binding properties. To evaluate whether conformational dynamics should be considered as relevant to ligand dissociation, we monitored the dynamics of a classic drug target, DHFR, that is known to undergo extensive motions on the µs-ms timescale. The wide range of affinities of the eight inhibitor complexes studied elicited a variety of dynamic behavior in the enzyme, and therefore this constitutes a *dynamics* structure-activity relationship (DSAR). This is distinct from, yet complementary to, flexibility-activity relationships (FAR), which focuses on dynamics of the bound ligand as shown previously for peptide ligands of Pin1[25]. Our results underscore the benefits of using a series of ligands to extract a kinetic relationship between internal motion and dissociation. A similar benefit from use of a ligand series was demonstrated recently for correlating ps-ns dynamics with conformational entropy in the case of calmodulin[26].

Here we show that, for a series of homologous antifolates binding to DHFR, binding affinity (K_i) is determined largely by k_{off}. We also demonstrate from CPMG relaxation dispersion measurements that the rate of millisecond-timescale internal motions in the enzyme ($k_{conf,forward}$) is related to both binding affinity and k_{off} for the series. Specifically, the correlation of $k_{conf,forward}$ to k_{off} provides evidence that internal protein motion is a mechanical initiator of ligand dissociation. Analysis of chemical shifts suggests that DHFR samples an identical excited state in solution regardless of which particular antifolate is bound, and that this state is novel because it differs from the excited states observed in the absence of ligand and in physiological complexes (Supplementary Fig. 4j). It is also worth noting that the THQ complexes undergo switching ~3 times faster than the physiological complexes. Because ligand is bound in the excited state and the rates of internal motion correlate with k_{off}, we propose that this excited state is en route to dissociation of inhibitor and $k_{conf,forward}$ provides an upper limit to k_{off}.

In previous work, connections between internal motions and protein activity have been drawn when an internal switching rate precisely matches a macroscopic rate constant[8,14]. We show here, through the use of a homologous ligand series, that such matching is not required to mechanistically connect two functional events. Ligand dissociation is fundamental in macromolecular interactions, and insights into what stimulates dissociation have potentially broad implications for manipulating biological systems. The main insight revealed here is that dissociation can be driven by defined protein internal motion, presumably at the interface, rather than by a fully stochastic process. This inference of motions driving dissociation would seem to be expected for a buried binding site in which a 'lid' must open for release; however, in this particular case, the ligand binding site is exposed, and yet dissociation appears to not be stochastic.

At what point during the conformational sampling does release actually occur? The simplest model consistent with our data is the following conformational gating model:

$$[E \cdot L]_A \underset{k_{conf,rev}}{\overset{k_{conf,fwd}}{\rightleftharpoons}} [E \cdot L]_B \overset{k_{off,B}}{\rightarrow} E_B + L. \quad (2)$$
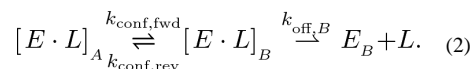
Upon transitioning to the excited state (state B), ligand remains initially bound but is subject to release while the gate is open, with rate constant $k_{off,B}$. In this model, release might depend on sub-millisecond motions that essentially kick out the ligand or break non-covalent interactions through shearing motions. Release from the open gate could also occur in a stochastic manner based on the overall strength of interactions (see below). Eqn. (2) is formally equivalent to the Linderstrom-Lang model for amide H/D exchange[27]. Hence, the overall rate constant for dissociation can be expressed[28] as $k_{off} = (k_{conf,fwd} \cdot k_{off,B})/(k_{conf,fwd} + k_{conf,rev} + k_{off,B})$, which can be rearranged to

$$k_{off,B} = \frac{1/K_{conf} + 1}{(1/k_{off} - 1/k_{conf,fwd})}, \quad (3)$$

in which $K_{conf} = k_{conf,fwd}/k_{conf,rev}$ and k_{off} is the bulk dissociation rate constant. Use of eqn. (3) yields values of $k_{off,B}$ ~25–100 times that of k_{off}, indicating significantly faster dissociation from the excited state (Supplementary Table 5) compared to the rate obtained when assuming simple dissociation from the ground state. We note that this gating model excludes ligand rebinding and hence is consistent with kinetic decay experiments. Rebinding may occur via different structures/mechanisms since the antifolate excited state is not observed in the holoenzyme (DHFR:NADPH, see Figure S4j).

What is somewhat surprising from the correlation of $k_{conf,forward}$ to K_i and k_{off} is that the relationship is log-linear. It follows that DHFR is not productive at releasing inhibitors each time it reaches the excited state, as $k_{conf,forward}$ is always greater than k_{off}. Thus, the enzyme appears to be more efficient at release as the rate of internal motion increases. Within the gating model, this may be explained by a loss of substituents. Adding substituents to the ring beyond the 2,4-diaminopyrimidine scaffold (e.g., methyls in THQ series, methoxy groups in TMP, etc.) could have a dual effect on the steps shown in eqn. (2): (i) these groups could serve to slow switching, as observed, due to stabilization of both ground and excited states, and (ii) by providing additional contacts to protein, these substituents would reduce the probability of stochastic release from the excited state, as observed (Fig. 4b, Table 1). Overall, the lack of a true linear relationship indicates an additional process (beyond the conformational change detected here) is associated with the final release of ligand.

An important caveat is that any ligand bearing resemblance to the series (or that binds to the same active site) should not necessarily obey the correlation in Figure 4b. Indeed, **2** and **4** do not (see Supplementary Results). It is reasonable to expect that numerous mechanisms for ligand release could compete with one another, and some ligands may trigger specific mechanisms over others due to their chemical structure. We have been fortunate here in using a panel of ligands that share a common mechanism that is distinct from release of folate-derived ligands. It will be interesting to see whether other ligand series against different proteins show similarity in behavior as was observed here.

Gaining an understanding of the molecular basis of k_{off} has implications for structure-based drug design. If protein dynamics are found to correlate with k_{off} in other systems, this type of analysis may be useful in optimizing ligand residence times to meet the desired pharmaceutical modulation of disease states. The DSAR methodology provides more than just a correlation between the rate of internal motions and k_{off} – it also potentially provides structural information on residues sampling multiple conformations and even what the structure of the excited state(s) may be[29–30]. This combined information would be useful in directing medicinal chemistry efforts toward modulating the stability of excited states that promote efficient ejection of inhibitors.

METHODS

Synthesis of (6-methyl-5,6,7,8-tetrahydroquinazoline-2,4-diamine) (compound 3)

Compound **3** was prepared by a one-step condensation reaction, similar to that described previously[31]. Briefly, dicyandiamide (10.19 g, 0.12 moles) and 4-methylcyclohexanone (11.33 g, 0.10 moles) were combined in a round bottom flask fitted with a Dean-Stark trap

and a condenser. The reaction was heated in an oil bath at 180 °C for three hours. Boiling water was added to the reaction as it was transferred to a separatory funnel for extraction. The desired compound was extracted from the aqueous layer with hot chloroform. The chloroform washes were dried over anhydrous magnesium sulfate before solvent was removed via rotary evaporation. A golden yellow liquid with white precipitate remained. Additional white solid was precipitated via addition of hexanes to the yellow liquid. The solid was isolated via filtration.

Synthetic procedures for **2** and **4–6** follow from that described above (Supplementary Methods). Spectroscopic data for all five compounds is summarized in Supplementary Methods. The enantiomers of **3** were separated on a Thar Investigator analytical/semi-preparative SFC. Purification was carried out using 20% isopropyl alcohol (0.1% diethylamine) in CO_2 with a CHIRALPAK IC column from Chiral Technologies.

K_i determination

As described previously, biochemical competition assays using a 96-well plate reader were used to determine the inhibition constant (K_i) for **2–6**[13,15]. The decrease in absorbance at 340 nm was monitored over time in a 2D titration of inhibitor and substrate.

Protein expression and purification

Isotopically labeled wild-type *E. coli* DHFR was over-expressed and purified as described previously[12]. Purified apo-DHFR was flash frozen, lyophilized, and stored in a desiccator at 4 °C until use.

NMR Spectroscopy

For ternary inhibitor complexes, samples contained 1 mM DHFR in NMR buffer (70 mM HEPES, 20 mM KCl, 1 mM EDTA, 1 mM DTT [pH 7.6]), 15 mM NADPH, 2.5–10 mM antifolate (E:NADPH:**2** – 10 mM; E:NADPH:**3** – 2.5 mM, E:NADPH:**4** – 8–10 mM; E:NADPH:**5** – 10 mM; E:NADPH:**6** – 10 mM), 10 mM glucose-6-phosphate, 10 U glucose-6-phosphate dehydrogenase, and 10% D_2O for spectrometer locking purposes. All samples were protected from light and air exposure by containment in amber NMR tubes flame-sealed under argon. Stock solutions of **2–6** were prepared in 10% D_2O/H_2O and PULCON was used to determined the concentration of each stock, relative to either valine or trimethoprim standards[32]. NMR experiments were performed as described previously, using both room temperature (500, 600, and 700 MHz) and cryogenic (500 and 700 MHz) probes[12–13]. NMRPipe was used to process NMR data, and data visualization was accomplished with the combination of NMRDraw and NMRView[33–34]. Refer to Supplementary Methods for further experimental details on assignment and relaxation experiments.

CPMG relaxation dispersion—[15]N CPMG relaxation dispersion experiments were conducted on highly deuterated (>80%) DHFR for the E:NADPH:**2** and **4–6** complexes while protonated DHFR was used for E:NADPH:**3**. Complexes with bound **2–4** were examined using a TROSY relaxation dispersion experiment at 700 MHz with a room temperature probe. Data collection at 700 MHz for complexes with bound **5–6** utilized a

cold probe and the regular non-TROSY experiment. Collection and analysis of the data was completed as described previously[12–13].

For group fits, all residues in a particular complex exhibiting significant μs-ms motion (excluding the C-terminal residues, see Supplementary Table 3) were grouped together, following the method of Mulder et al[22]. Single k_{ex} and p_A values were fit for a group, whereas ω values were fit in a residue-specific manner. Residues found to have a significantly improved local fit relative to the group fit (i.e., having a $\chi_{2group}/\chi_{2local}$ ratio of > 2) are reported with ω values from the local fit instead of the group fit. Although it is possible that multiple groups with slightly different exchange parameters exist for individual complexes, because such differences are small in most complexes, they cannot be easily resolved and the simplest case of a single group was used. In the case of E:NADPH:**2** and E:NADPH:**4**, single-group fits of all residues together would not converge. Upon removal of four residues with increased local k_{ex} values (37, 50, 54, and 58), group fitting for E:NADPH:**4** converged and the residues appeared to fit together based on χ^2 ratios. This same approach for E:NADPH:**2** resulted in convergence (40, 44, 48, 50, 54, 57, 98, 115, and 119 removed); however, the residues did not group well together based on χ^2 ratios. Group fits for complexes with bound **2** and **4** are reported, but it should be noted that the fits were not conducted in the same fashion as for the rest of the series. One interesting point to mention is that E:NADPH:**2** and E:NADPH:**4** resulted in similar group fitting for both the 'slow' and 'fast' moving sets of residues. We speculate that the similar placement of the methyl substituent in these two inhibitors may underlie why they appear to cause faster switching motions in DHFR. Also, for inhibitors **2** and **4**, the possibility that both *R* and *S* enantiomers bind could also result in different switching than for the remainder of the series, although this appears not to be the case for **6**.

The sign of ω was determined from peak positions in HSQC and HMQC spectra[35]. Sign determination for ω was completed on six of the eight ternary complexes (E:NADPH:**2** and E:NADPH:**4** excluded). Given the strong pattern of ω sign observed for the antifolate consensus residues (Fig. 4d), the signs for the complexes with **2** and **4** were assumed to agree with the pattern. Additionally, the sign of ω determined for the three other THQ compounds (**3**, **5–6**) should be representative of **2** and **4**. Fitted parameters and the sign of ω are summarized for each complex in Supplementary Results.

Protein crystallization and structure determination

Crystals of E:NADPH:**3**, E:NADPH:**4**, and E:NADPH:**5** were grown using similar conditions as described previously[13,17,36]. See Supplementary Methods and Results for details of crystallization, data collection, and structure refinement.

Determination of k_{off}

A fluorescence competitive binding assay, as described previously, was used to determine k_{off} for **2–6** from the E:NADPH holoenzyme[13,37]. Refer to Supplementary Methods for a detailed methods description.

Supplementary Material

Refer to Web version on PubMed Central for supplementary material.

Acknowledgments

References

1. Tummino PJ, Copeland RA. Residence time of receptor-ligand complexes and its effect on biological function. Biochemistry. 2008; 47:5481–5492. [PubMed: 18412369]

2. Lu H, Tonge PJ. Drug-target residence time: critical information for lead optimization. Curr Opin Chem Biol. 2010; 14:467–474. [PubMed: 20663707]

3. Olson JS, Phillips GN Jr. Kinetic pathways and barriers for ligand binding to myoglobin. J Biol Chem. 1996; 271:17593–17596. [PubMed: 8698688]

4. Bourgeois D, et al. Complex landscape of protein structural dynamics unveiled by nanosecond Laue crystallography. Proc Natl Acad Sci U S A. 2003; 100:8704–8709. [PubMed: 12847289]

5. Bourne HR, Sanders DA, McCormick F. The GTPase superfamily: conserved structure and molecular mechanism. Nature. 1991; 349:117–127. [PubMed: 1898771]

6. Ishima R, Freedberg DI, Wang YX, Louis JM, Torchia DA. Flap opening and dimer-interface flexibility in the free and inhibitor-bound HIV protease, and their implications for function. Structure. 1999; 7:1047–1055. [PubMed: 10508781]

7. Eisenmesser EZ, et al. Intrinsic dynamics of an enzyme underlies catalysis. Nature. 2005; 438:117–121. [PubMed: 16267559]

8. Boehr DD, McElheny D, Dyson HJ, Wright PE. The dynamic energy landscape of dihydrofolate reductase catalysis. Science. 2006; 313:1638–1642. [PubMed: 16973882]

9. Labeikovsky W, Eisenmesser EZ, Bosco DA, Kern D. Structure and dynamics of pin1 during catalysis by NMR. J Mol Biol. 2007; 367:1370–1381. [PubMed: 17316687]

10. Masterson LR, et al. Dynamics connect substrate recognition to catalysis in protein kinase A. Nat Chem Biol. 6:821–828. [PubMed: 20890288]

11. Sapienza PJ, Mauldin RV, Lee AL. Multi-timescale dynamics study of FKBP12 along the rapamycin-mTOR binding coordinate. J Mol Biol. 405:378–394. [PubMed: 21073880]

12. Mauldin RV, Carroll MJ, Lee AL. Dynamic Dysfunction in Dihydrofolate Reductase Results from Antifolate Drug Binding: Modulations of Dynamics within a Structural State. Structure. 2009; 17:386–394. [PubMed: 19278653]

13. Carroll MJ, et al. Direct detection of structurally resolved dynamics in a multi-conformation receptor-ligand complex. J Am Chem Soc. 2011; 133:6422–6428. [PubMed: 21469679]

14. Eisenmesser EZ, Bosco DA, Akke M, Kern D. Enzyme dynamics during catalysis. Science. 2002; 295:1520–1523. [PubMed: 11859194]

15. Zolli-Juran M, Cechetto JD, Hartlen R, Daigle DM, Brown ED. High throughput screening identifies novel inhibitors of Escherichia coli dihydrofolate reductase that are competitive with dihydrofolate. Bioorg Med Chem Lett. 2003; 13:2493–2496. [PubMed: 12852950]

16. Matthews DA, et al. Dihydrofolate reductase: x-ray structure of the binary complex with methotrexate. Science. 1977; 197:452–455. [PubMed: 17920]

17. Sawaya MR, Kraut J. Loop and Subdomain Movements in the Mechanism of *Escherichia coli* Dihydrofolate Reductase: Crystallographic Evidence. Biochemistry. 1997; 36:586–603. [PubMed: 9012674]

18. Loria JPRM, Palmer AG. A relaxation-compensated Carr-Purcell-Meiboom-Gill sequence for characterizing chemical exchange by NMR spectroscopy. J Am Chem Soc. 1999; 121:2331–2332.

19. Boehr DD, McElheny D, Dyson HJ, Wright PE. Millisecond timescale fluctuations in dihydrofolate reductase are exquisitely sensitive to the bound ligands. Proc Natl Acad Sci U S A. 2010; 107:1373–1378. [PubMed: 20080605]

20. Palmer AG 3rd, Kroenke CD, Loria JP. Nuclear magnetic resonance methods for quantifying microsecond-to-millisecond motions in biological macromolecules. Methods Enzymol. 2001; 339:204–238. [PubMed: 11462813]

21. Osborne MJ, Venkitakrishnan RP, Dyson HJ, Wright PE. Diagnostic chemical shift markers for loop conformation and substrate and cofactor binding in dihydrofolate reductase complexes. Protein Sci. 2003; 12:2230–2238. [PubMed: 14500880]

22. Mulder FA, Mittermaier A, Hon B, Dahlquist FW, Kay LE. Studying excited states of proteins by NMR spectroscopy. Nat Struct Biol. 2001; 8:932–935. [PubMed: 11685237]

23. Baccanari DP, Joyner SS. Dihydrofolate reductase hysteresis and its effect of inhibitor binding analyses. Biochemistry. 1981; 20:1710–1716. [PubMed: 7013798]

24. Appleman JR, Howell EE, Kraut J, Kuhl M, Blakley RL. Role of aspartate 27 in the binding of methotrexate to dihydrofolate reductase from Escherichia coli. J Biol Chem. 1988; 263:9187–9198. [PubMed: 3288632]

25. Namanja AT, et al. Toward flexibility-activity relationships by NMR spectroscopy: dynamics of Pin1 ligands. J Am Chem Soc. 2010; 132:5607–5609. [PubMed: 20356313]

26. Frederick KK, Marlow MS, Valentine KG, Wand AJ. Conformational entropy in molecular recognition by proteins. Nature. 2007; 448:325–329. [PubMed: 17637663]

27. Berger A, Linderstrom-Lang K. Deuterium exchange of poly-DL-alanine in aqueous solution. Arch Biochem Biophys. 1957; 69:106–118. [PubMed: 13445185]

28. Hvidt A, Nielsen SO. Hydrogen exchange in proteins. Adv Protein Chem. 1966; 21:287–386. [PubMed: 5333290]

29. Hansen DF, Vallurupalli P, Kay LE. Using relaxation dispersion NMR spectroscopy to determine structures of excited, invisible protein states. J Biomol NMR. 2008; 41:113–120. [PubMed: 18574698]

30. Hansen DF, Vallurupalli P, Lundstrom P, Neudecker P, Kay LE. Probing chemical shifts of invisible states of proteins with relaxation dispersion NMR spectroscopy: how well can we do? J Am Chem Soc. 2008; 130:2667–2675. [PubMed: 18237174]

31. Gangjee A, Zaveri N, Queener SF, Kisliuk RL. Synthesis and Biological Activities of Tetrahydroquinazoline Analogs of Aminopterin and Methotrexate. Journal of Heterocyclic Chemistry. 1995; 32:243–247.

32. Wider G, Dreier L. Measuring protein concentrations by NMR spectroscopy. J Am Chem Soc. 2006; 128:2571–2576. [PubMed: 16492040]

33. Delaglio F, et al. NMRPipe - a multidimensional spectral processing system based on Unix pipes. J Biomol NMR. 1995; 6:277–293. [PubMed: 8520220]

34. Johnson BA, Blevins RA. NMRView - a computer program for the visualization and analysis of NMR data. J Biomol NMR. 1994; 4:603–614. [PubMed: 22911360]

35. Skrynnikov NR, Dahlquist FW, Kay LE. Reconstructing NMR spectra of "invisible" excited protein states using HSQC and HMQC experiments. J Am Chem Soc. 2002; 124:12352–12360. [PubMed: 12371879]

36. Summerfield RL, et al. A 2.13 A Structure of *E. coli* Dihydrofolate Reductase Bound to a Novel Competitive Inhibitor Reveals a New Binding Surface Involving the M20 Loop Region. J Med Chem. 2006; 49:6977–6986. [PubMed: 17125251]

37. Fierke CA, Johnson KA, Benkovic SJ. Construction and evaluation of the kinetic scheme associated with dihydrofolate reductase from Escherichia coli. Biochemistry. 1987; 26:4085–4092. [PubMed: 3307916]
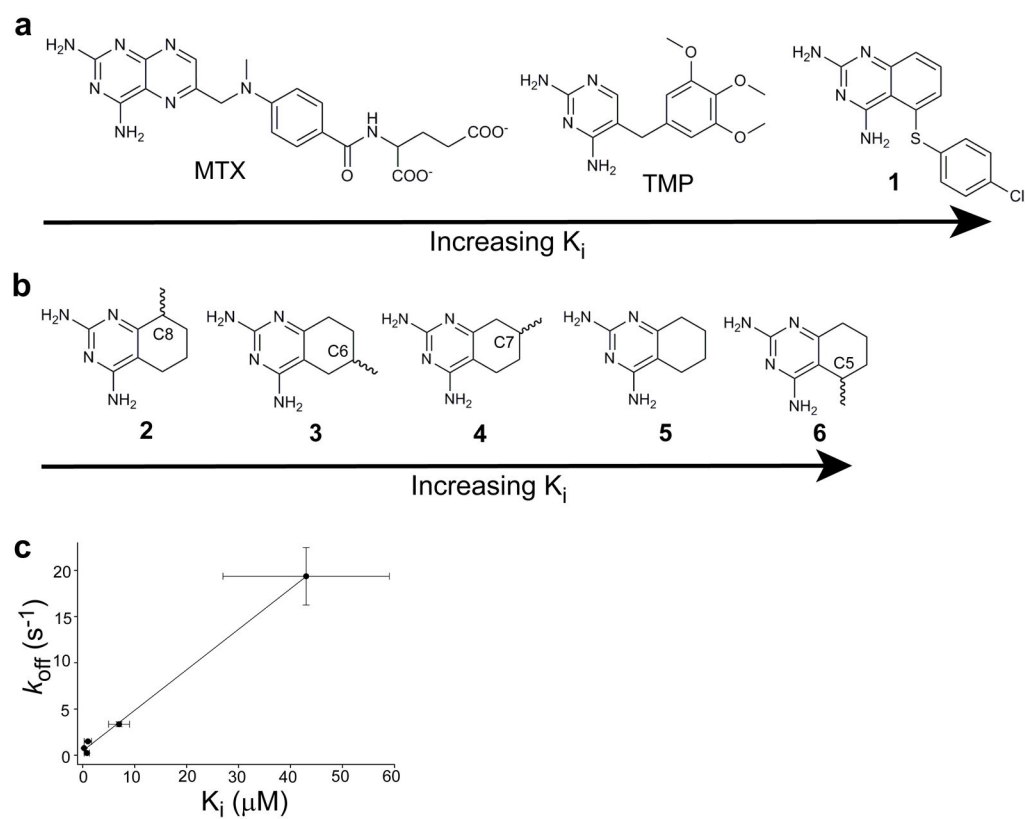
Figure 1.
The series of reduced-affinity and previously characterized antifolates. (a) Chemical structures of the previously characterized antifolates – methotrexate (MTX), trimethoprim (TMP), and **1**. (b) Chemical structures of the reduced-affinity antifolates **2–6**. (c) The relationship between k_{off} and K_i for the series of reduced-affinity antifolates ($R = 0.99$).
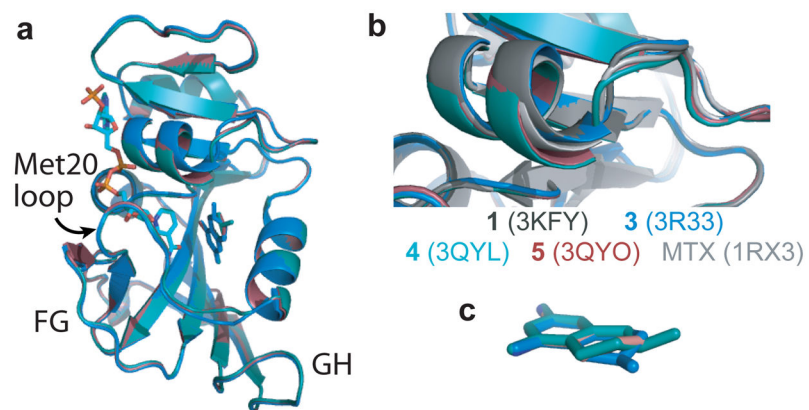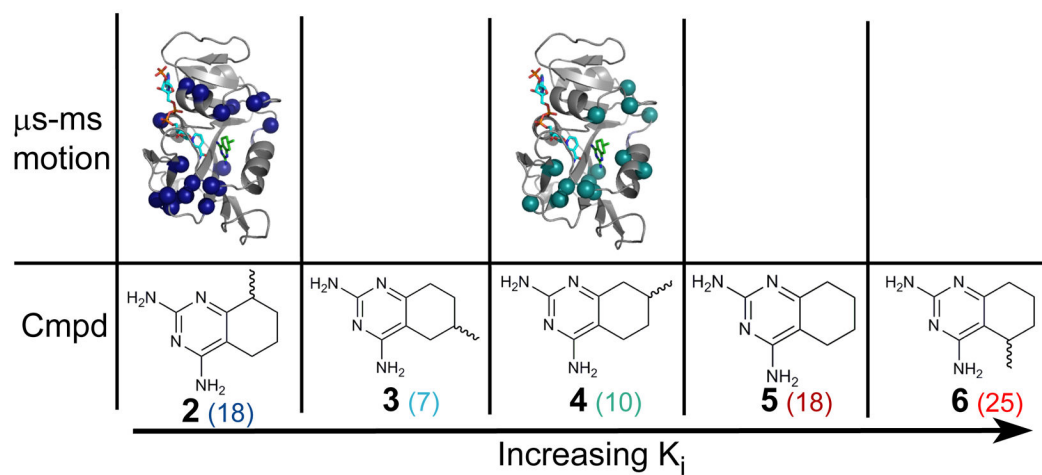
Figure 2.
High resolution crystal structures for the series. (a) Overlay of the crystal structures for E:NADPH:**3** (blue), ENADPH:**4** (teal), and E:NADPH:**5** (maroon). NADPH is shown in cyan and bound antifolate in the colors designated per complex. (b) Expansion of the C-helix, now overlaying five inhibitor-bound complexes (E:NADPH:**1** in dark grey and E:NADPH:MTX in light grey). PDB IDs are listed parenthetically. (c) Differential puckering of the saturated ring in the bound inhibitors, colored as in (a).

Figure 3.
Slow timescale dynamics for the reduced-affinity inhibitor series. Sites along the backbone with detectable µs-ms motion are highlighted in colored spheres for each complex, ordered from left to right by increasing K_i value. The number of residues with significant R_{ex} is given parenthetically.
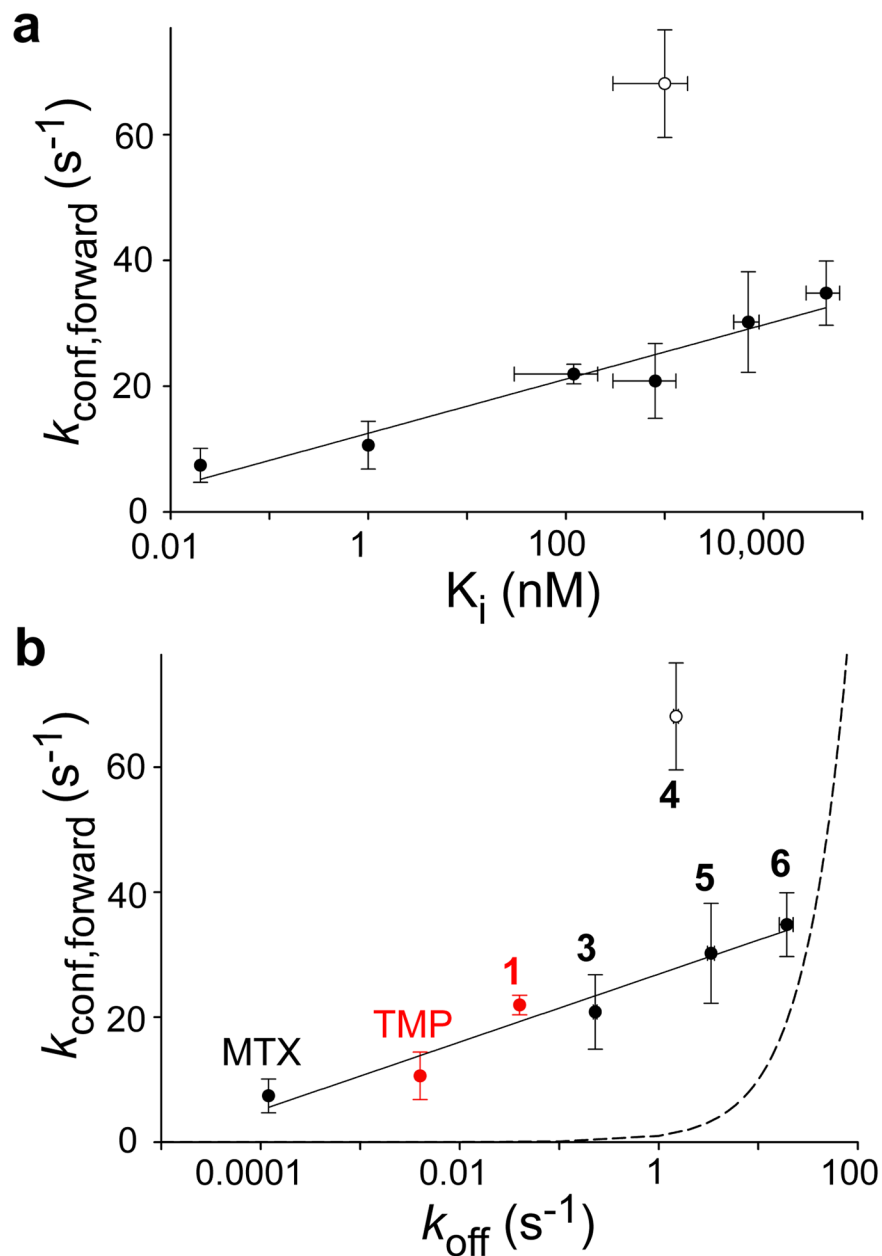
Figure 4.
Internal motions vary with K_i and k_{off}. (a) The forward rate of motion ($k_{conf,forward}$) fit from relaxation dispersion data for each complex varies exponentially with the K_i value for the bound inhibitor ($R = 0.97$). The open circle represents the best fit for E:NADPH:**4**. (b) An exponential correlation is also seen between $k_{conf,forward}$ and k_{off} ($R = 0.97$). Data points in red have predicted k_{off} values, as described in the text. k_{off} for TMP and **1** were calculated based on estimated values for k_{on}. For **1**, the average k_{on} for the THQ series was used. For TMP, because of its greater similarity to MTX, k_{on} was taken to be intermediate between MTX and the average value for the THQ series. The data point for E:NADPH:**4** (unfilled circle) does not fall along this exponential correlation, suggesting that this correlation may

not always be predictive. The dashed curve represents what would be expected if the correlation were linear. Error bars represent standard deviations (originating from Monte Carlo simulations in the case of $k_{conf,forward}$).
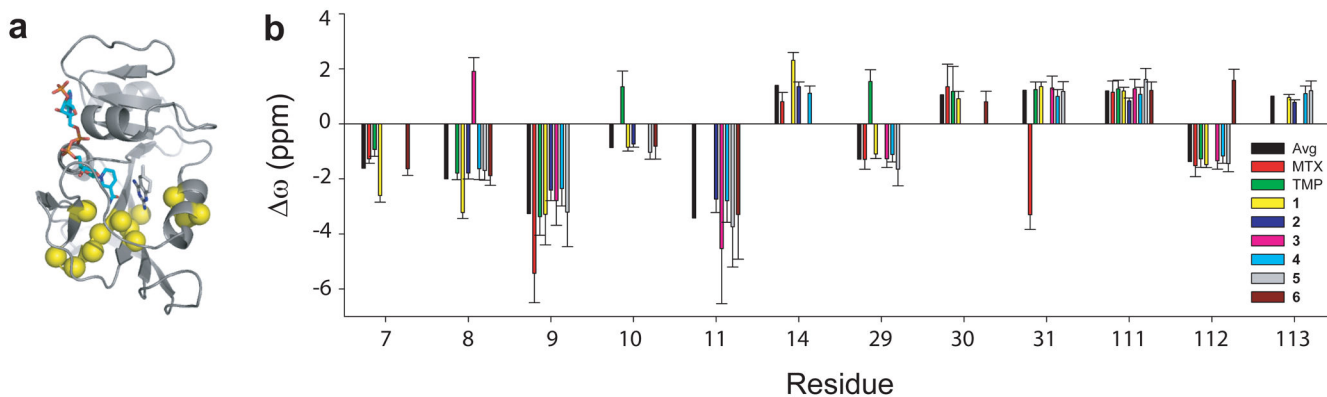
Figure 5.
Antifolate consensus sites sample a structurally similar excited state. (a) The twelve antifolate consensus sites are highlighted in yellow colored spheres. (b) Dynamic ω values fitted from relaxation dispersion for these twelve sites cluster for each residue. The eight complexes are colored by the bound inhibitor, as indicated in the legend. Averages were calculated only from residues that have the dominant sign. No bar is shown if that residue did not exhibit significant slow motion while bound to a particular inhibitor. Error bars result from standard deviations derived from Monte Carlo simulations.

Table 1

Binding affinities, kinetic off-rates, and relaxation dispersion group-fitted parameters for the series of antifolates.

Cmpd	K_i (μM)	k_{off} (s^{-1})	k_{ex} (s^{-1})	P_A (%)	$k_{conf,forward}$ (s^{-1})
MTX	0.000021[a]	0.00010[b]	425 ± 154[c]	98.2 ± 0.4[c]	7.4 ± 2.7[c]
TMP	0.0012[a]	0.004[d]	459 ± 165[c]	97.7 ± 0.4[c]	10.6 ± 3.8[c]
1	0.12 ± 0.009[e]	0.04[d]	844 ± 59[e]	97.4 ± 0.1[e]	21.9 ± 1.6[e]
2	0.23 ± 0.03[f]	0.76 ± 0.05[f]	1659 ± 168[g]	95.9 ± 1.0[g]	68.0 ± 7.6[g]
3	0.8 ± 0.5[f]	0.23 ± 0.01[f]	1041 ± 292	98 ± 0.5	20.8 ± 6.0
4	1 ± 0.7[f]	1.49 ± 0.08[f]	1841 ± 189[h]	96.3 ± 2.2[h]	68.1 ± 8.6[h]
5	7 ± 2	3.35 ± 0.27	1448 ± 423	97.9 ± 1.0	30.4 ± 9.2
6	43 ± 16[f]	19.37 ± 3.11[f]	1515 ± 206	97.7 ± 1.1	34.8 ± 5.1

[a] Values taken from the literature[23].

[b] Value taken from literature[24].

[c] Previously published values[12].

[d] Values calculated from K_i and k_{on}, as described in the text.

[e] Previously published values[13].

[f] Values reported as apparent K_i or k_{off} values, since compounds **2**, **3**, **4**, and **6** are racemic mixtures.

[g] Sites were split into two groups. The best fit for the slower group is given, despite the observation that many sites possess high χ^2 ratios.

[h] Sites were split into two groups. The best fit for the slower group is given. All residues 'fit' well into this group based on χ^2 ratios.